Published in final edited form as:
Cell Metab. 2012 February 8; 15(2): 186–200. doi:10.1016/j.cmet.2012.01.009.

Mitochondrial Fission Triggered by Hyperglycemia Is Mediated by ROCK1 Activation in Podocytes and Endothelial Cells

Wenjian Wang[1,*], **Yin Wang**[1,*], **Jianyin Long**[1], **Jinrong Wang**[1], **Sandra B. Haudek**[2], **Paul Overbeek**[3], **Benny H.J. Chang**[3], **Paul T. Schumacker**[4], and **Farhad R. Danesh**[1,5]

[1]Department of Medicine-Nephrology, Baylor College of Medicine, Houston, TX

[2]Department of Medicine-Division of Cardiovascular Sciences, Baylor College of Medicine, Houston, TX

[3]Department of Molecular and Cellular Biology, Baylor College of Medicine, Houston, TX

[4]Department of Pediatrics, Feinberg School of Medicine, Northwestern University, Chicago, IL

[5]Department of Pharmacology, Baylor College of Medicine, Houston, TX

SUMMARY

Several lines of evidence suggest that mitochondrial dysfunction plays a critical role in the pathogenesis of microvascular complications of diabetes, including diabetic nephropathy. However, the signaling pathways by which hyperglycemia leads to mitochondrial dysfunction are not fully understood. Here we examined the role of Rho-associated coiled-coil containing protein kinase 1 (ROCK1) on mitochondrial dynamics by generating two diabetic mouse models with targeted deletions of ROCK1, and an inducible podocyte-specific knock-in mouse expressing a constitutively active (cA) mutant of ROCK1. Our findings suggest that ROCK1 mediates hyperglycemia-induced mitochondrial fission by promoting dynamin-related protein-1 (Drp1) recruitment to the mitochondria. Deletion of ROCK1 in diabetic mice prevented mitochondrial fission, whereas podocyte-specific cA-ROCK1 mice exhibited increased mitochondrial fission. Importantly, we found that ROCK1 triggers mitochondrial fission by phosphorylating Drp1 at Serine 600 residue. These findings provide insights into the unexpected role of ROCK1 in a signaling cascade that regulates mitochondrial dynamics.

INTRODUCTION

Diabetes is the most common metabolic disease in the world and a leading cause of blindness, end-stage renal disease, and non-traumatic loss of limb. Although there is considerable evidence suggesting that chronic hyperglycemia is the main culprit for microvascular complications of diabetes, the underlying molecular mechanism of diabetic complications remains poorly understood. Using cultured aortic endothelial cells, Nishikawa

Corresponding Author: Farhad R. Danesh M.D., Departments of Medicine & Pharmacology, Division of Nephrology, Baylor College of Medicine, Houston, Texas, 77030, USA, Phone: 713-798-1304, Fax: 713-798-5010, danesh@bcm.edu.
*Both authors contributed equally to the manuscript.

SUPPLEMENTAL INFORMATION

Supplemental information includes seven figures, Supplemental Experimental Procedures and Supplemental References.

et al. (Nishikawa et al., 2000) provided experimental evidence that hyperglycemia leads to overproduction of reactive oxygen species (ROS), which was then prevented by overexpression of uncoupling protein-1 and manganese superoxide dismutase. These observations have led to the "unifying hypothesis" whereby increased mitochondrial ROS production was proposed to serve as the common link for several key pathogenic pathways involved in microvascular complications of diabetes (Brownlee, 2001; Nishikawa et al., 2000). However, the specific signaling molecules which couple hyperglycemia with mitochondrial ROS production, and the nature of mitochondrial dysfunction associated with cell apoptosis in the diabetic milieu remain to be defined.

Rho-associated coiled-coil containing protein kinase (ROCK) is a downstream effector of RhoA, that is believed to play a key role in mediating the effects of RhoA on stress fiber formation, ROS production, and cellular apoptosis (Noma et al., 2008; Ongusaha et al., 2008; Riento and Ridley, 2003). We have previously shown that pharmacological inhibition of ROCK by fasudil ameliorates albuminuria and progression of diabetic nephropathy (DN) in an established mouse model of diabetes (Kolavennu et al., 2008). Other laboratories have reported complementary data, suggesting that the ROCK pathway may play an important role in the pathogenesis of DN (Gojo et al., 2007; Kikuchi et al., 2007; Peng et al., 2008). However, fasudil is not a selective inhibitor of ROCK, and it may inhibit other serine/threonine kinases such as protein kinases A and C (PKA, PKC) at high concentrations (Davies et al., 2000; Sasaki et al., 2002). Moreover, the use of fasudil cannot distinguish the individual roles of the two isoforms of ROCK, ROCK1 and ROCK2, in the progression of DN. Importantly, despite an emerging role for ROCK in DN, the underlying molecular mechanisms for its pathogenic effect are unknown. To address these questions, in the current study we tested the hypothesis that ROCK1 activation promotes progression of DN by triggering mitochondrial dysfunction.

Mitochondrial dynamics have emerged as an important process that contributes to mitochondrial dysfunction in a variety of metabolic conditions, including in the diabetic milieu (Yu et al., 2006). Mitochondria are dynamic organelles that frequently change their shape, number, and intracellular distribution in response to fluctuations in metabolic demands. Under physiological conditions, mitochondria are elongated and filamentous, but they undergo extensive fragmentation during apoptosis (Youle and Karbowski, 2005). Several studies have indicated that excessive mitochondrial fission is associated with increased ROS production and cellular apoptosis (Tanaka and Youle, 2008; Youle and Karbowski, 2005). Interestingly, *in vitro* studies have also implicated mitochondrial fission as a key mediator of increased ROS production and cellular apoptosis under hyperglycemic conditions (Rube and van der Bliek, 2004; Yu et al., 2006). However, these studies have been limited to tissue culture cells and the precise role of mitochondrial dynamics in the diabetic milieu and its complications *in vivo* remain to be explored.

Here we report that ROCK1 plays a critical role in progression of DN by triggering mitochondrial fission, which results in recruitment of dynamin-related protein-1 (Drp1) to the mitochondria. Thus, our findings identify ROCK1 as a potent regulator of mitochondrial dynamics, and shed light into the critical role of ROCK1 in progression of DN.

RESULTS

Albuminuria Is Markedly Decreased in Mice Lacking ROCK1 in Several Experimental Models of Diabetes

We generated two diabetic mice models with targeted deletion of ROCK1 to assess the specific role of ROCK1 in DN. First, we used ROCK1-null (ROCK1$^{-/-}$) and *Lepr*$^{db/+}$ mice to generate diabetic *Lepr*$^{db/db}$ ROCK1$^{-/-}$ mice (hereafter referred to as db/db:ROCK1$^{-/-}$).

Western blotting confirmed absence of ROCK1 protein in the kidney, heart and spleen (Figure 1A). Four groups of mice were investigated: db/+:ROCK1$^{+/+}$, db/+:ROCK1$^{-/-}$, diabetic db/db:ROCK1$^{+/+}$, and diabetic db/db:ROCK1$^{-/-}$ mice. Basic parameters, including systolic blood pressure, body weight, kidney weight, plasma glucose, and urinary albumin excretion were determined for each animal. Comparison of the non-diabetic ROCK1 knockout mice with their control wild-type littermates showed that the knockout animals did not differ significantly from wild type in any of these parameters, which is in general agreement with previous reports (Chang et al., 2006; Haudek et al., 2009; Zhang et al., 2006). Double mutant diabetic mice (db/db:ROCK1$^{-/-}$) were similar to diabetic db/db:ROCK1$^{+/+}$ mice for blood pressure, body weight, kidney weight/body weight, and serum glucose levels (Figures 1B, 1C, 1D, 1E, 1F, and 1G), However, a marked reduction in the urinary albumin excretion was observed in the diabetic db/db:ROCK1$^{-/-}$ mice compared with that in db/db:ROCK1$^{+/+}$ mice at 16-weeks of age (346±106 *vs.* 227±106 μg/mg, $p<0.05$) (Figure 1H). Consistent with the biochemical changes in the urine, Periodic Acid-Schiff (PAS) staining also revealed a significant reduction in mesangial matrix expansion in db/db:ROCK1$^{-/-}$ mice compared with that in db/db:ROCK1$^{+/+}$ diabetic mice by 24 weeks of age (Figure 1I). Furthermore, the glomerular basement membrane thickness was reduced (Figure 1J), and the loss of podocytes was prevented in db/db: ROCK1$^{-/-}$ mice (Figure 1K).

To evaluate the consequences of targeted deletion of ROCK1 in a different model of DN, ROCK1$^{+/+}$ and ROCK1$^{-/-}$ mice were made diabetic with streptozotocin (STZ). Since we used a high dose of STZ to induce proteinuria (Chow et al., 2006), diabetic mice were monitored for 16–24 weeks after STZ injections to avoid potential acute kidney injury associated with STZ administration in the first 6–8 weeks. Our findings indicate that diabetic ROCK1$^{-/-}$ and ROCK1$^{+/+}$ mice exhibited similar weights, blood pressure, and blood glucose levels 16 weeks post STZ injection, but knockout of ROCK1 prevented the marked increase in the diabetes-induced kidney weight/body weight ratio (Figures 2A, 2B, 2C, and 2D). Importantly, the increase in the urinary albumin excretion and enhanced mesangial matrix expansion observed in diabetic control mice after 16 weeks of hyperglycemia were prevented in diabetic ROCK1$^{-/-}$ mice (Figure 2E, 2F). Furthermore, consistent with a renoprotective effect of ROCK1$^{-/-}$, the glomerular basement membrane thickness and podocyte numbers were preserved in diabetic ROCK1$^{-/-}$ mice (Figures 2G, 2H). Taken together, these results demonstrate a critical role of ROCK1 activation in DN, and suggest that targeted deletion of ROCK1 is renoprotective in both type 1 and type 2 models of diabetes.

Inducible Cre-Recombinase Activation of Podocyte-Specific cA-ROCK1 Bitransgenic Mice Causes Albuminuria

To understand the role of ROCK1 overexpression in the development of albuminuria, we generated a conditionally inducible knock-in of constitutively active (cA) ROCK1 by targeting cA-ROCK1 into the ROSA 26 locus through homologous recombination. The strategy for generating cA-ROCK1 knock-in mouse is shown in Figure 3A. We generated a targeting vector carrying the cA-human ROCK1 mutant, and a transcriptional stop cassette flanked by *LoxP* recombination sites upstream of the cA-ROCK1 coding region to maintain the allele silent until the introduction of Cre recombinase. Two transgenic mouse lines that showed germ line transmission of the transgene were selected and maintained for further studies. Offspring genotypes from heterozygous mating followed Mendelian frequencies. To investigate the role of ROCK1 specifically in podocytes, we crossed Rosa$^{cA\text{-}ROCK1}$ transgenic mice (Tg$^{cA\text{-}ROCK1flox/+}$) with an inducible podocyte-specific Cre transgenic line (Tg$^{podocin\text{-}iCreERT2/+}$) to generate single-copy cA-ROCK-1 overexpression in podocytes (Figure 3B). The podocyte-specific Cre line of transgenic mice which expresses iCreER^{T2} under the control of the podocin promoter was previously generated in our laboratory (Wang

et al., 2010). The use of iCreER^{T2} allowed us to control expression of floxed cA-ROCK1 in the presence of tamoxifen in a temporal-specific manner in podocytes. We generated mice that were heterozygous for the floxed cA-ROCK1 and carried the podocin-Cre transgene ($Tg^{cA\text{-}ROCK1flox/+}$;$Tg^{podocin\text{-}iCre/+}$), and then activated podocin-Cre by administrating tamoxifen to bitransgenic mice at a dose of 2 mg/day/mouse for a total of 10 injections by 8 weeks of age (Wang et al., 2010). The Cre-activated bitransgenic mice (hereafter referred to as podocin Cre cA-ROCK1) were indistinguishable in size from their control littermate mice ($Tg^{cA\text{-}ROCK1flox/+}$ or $Tg^{podocin\text{-}iCre/+}$, hereafter referred to as control mice) (Figure 3C). We assessed ROCK1 activation in the glomeruli of 15-week-old mice by isolating glomeruli from podocin Cre cA-ROCK1 mice 5 weeks after induction with tamoxifen (Figures S1-A, S1-B, and S1-C). ROCK1 activation assay revealed a ~3.5 fold increase of ROCK1 activation in the kidney glomeruli (Figure 3D), whereas it was unchanged in other tissues (Figure S1-D). Analysis of the inducible podocin Cre cA-ROCK1 mice showed significant increase in albuminuria (from 29±2 to 77±9 and 75±6 μg/mg, $p<0.05$) following 2 and 5 weeks of tamoxifen injection (Figure 3E), while no significant changes were observed on their blood pressure, body weight, blood glucose, and serum creatinine levels compared with their control littermates mice at 24 weeks of age (Figure 3F). Histologically, five weeks after induction, glomeruli from podocin Cre cA-ROCK1 mice exhibited increased mesangial matrix accumulation (Figure 3G). However, enhanced mesangial matrix was not observed consistently in all glomeruli. The main histological change was effacement of foot processes in podocytes in podocin Cre cA-ROCK1 mice on electron microscopy (Figure 3H). Furthermore, podocyte numbers were significantly reduced in podocin Cre cA-ROCK1 mice (Figure 3I). Taken together, these data demonstrate that podocyte-specific knock-in of cA-ROCK1 promotes albuminuria, podocytes effacement, and matrix expansion.

Deletion of ROCK1 Prevents Glomerular Apoptosis and Mitochondrial ROS Production in Vivo

We next explored the precise mechanisms for ROCK1-induced albuminuria. ROCK1 activation can induce apoptosis, and growing evidence has shown that mitochondrial ROS (mtROS) and apoptosis are critical in the pathogenesis of microvascular complications of diabetes, including DN (Coughlan et al., 2007; de Cavanagh et al., 2008; Kiritoshi et al., 2003; Nishikawa et al., 2000). Therefore, we tested the effect of ROCK1 on mtROS production in the glomeruli of control and STZ-induced diabetic mice. To specifically assess mitochondrial superoxide production, we performed Electron Paramagnetic Resonance (EPR) spectroscopy, and used 1-hydroxy-3-methoxycarbonyl-2,2,5,5-tetramethyl-pyrrolidine (CMH) as the spin trap (Piskernik et al., 2008; Pospisilik et al., 2007). We observed ~ 8-fold increase in the mtROS generation from the isolated kidney glomeruli of diabetic wild type mice, whereas this increase was prevented in diabetic ROCK1$^{-/-}$ mice (Figure 4A, **left panel**). The number of apoptotic cells and the caspase-3 activity within the glomeruli of diabetic ROCK$^{-/-}$ mice were also significantly reduced compared to that in wild type diabetic mice (Figure 4A, **middle and right panels**). Conversely, mtROS, frequency of apoptosis, and caspase-3 activity were all significantly increased in podocin Cre cA-ROCK1 mice (Figure 4B).

To elucidate the mechanisms by which deletion of ROCK1 can prevent cellular apoptosis, we carried out cell fractionation experiments to determine the effect of ROCK1 on the pro-apoptotic factors Bax and cytochrome *c*. Bax activation leads to its translocation to the outer mitochondrial membrane, where it can permeabilize the mitochondrial membrane by forming pores, allowing release of cytochrome *c*. We assessed Bax protein levels in the mitochondrial fractions, and found that ROCK1 deficiency led to significant decreases in the diabetic mice when compared with wild-type diabetic mice (Figure 4C). In contrast, mitochondrial levels of cytochrome *c* were significantly increased in diabetic ROCK1$^{-/-}$

mice (Figure 4C, **right panel**). Collectively, these data indicate that ROCK1 may be involved in increased mitochondrial superoxide production, and diabetic-induced cellular apoptosis in the kidney glomeruli.

ROCK1 Mediates Diabetic-Induced Mitochondrial Fission in Vivo

Recent published work indicates that mitochondrial fission couples mitochondrial ROS with cell apoptosis in hyperglycemic conditions (Yu et al., 2006). However, two important questions remain to be addressed. First, it is unclear whether ROCK1 mediates hyperglycemia-induced mitochondrial fission, and second, it remains unknown whether ROCK1 plays a role in the pathogenesis of DN. Thus, to uncover the effect of the diabetic milieu and ROCK1 on mitochondrial dynamics in the kidneys *in vivo*, we examined the mitochondrial morphology in the kidney glomeruli isolated from STZ-induced diabetic ROCK1$^{-/-}$ mice. In wild type (*wt*) diabetic mice, electron microscopy revealed increased mitochondrial fragmentation as evidenced by a significant increase in small, punctate mitochondria in podocytes compared to those in non-diabetic control mice, which exhibited long filamentous mitochondria (Figure 4D). However, the increased mitochondrial fragmentation in podocytes was prevented in diabetic ROCK1$^{-/-}$ mice. To quantify changes in mitochondrial fragmentation in podocytes, we determined the aspect ratio (AR) of mitochondria in each group (Brooks et al., 2007; Yu et al., 2006). Wild type diabetic mice exhibit ~50% reduction of the AR ratio in podocytes compared with that of non-diabetic control mice (Figure 4E). In contrast, the AR ratio in podocytes from diabetic ROCK1$^{-/-}$ was markedly improved and statistically significantly different from that in diabetic mice ($p<0.01$). To further assess mitochondrial fragmentation in diabetic podocytes, we performed 3D reconstruction of mitochondria from serial sections of EM micrographs. The mitochondria in *wt* diabetic mice were fragmented into short spheres. In contrast, podocytes from diabetic ROCK1$^{-/-}$ exhibited a typical tubular network of mitochondria by 3D EM (Figure 4F). Similar results were obtained in db/db:ROCK1$^{-/-}$ mice (Figures S2-A, and S2-B).

We next examined mitochondrial morphology in podocytes from podocin Cre cA-ROCK1 mice. We observed a significant increase in mitochondrial fission in these mice as suggested by a marked decrease in AR ratio (Figures 4G, and 4H). Furthermore, mitochondrial Bax (mtBax) levels were increased, whereas levels of mitochondrial cytochrome *c* were markedly reduced in the kidney glomeruli of podocin Cre cA-ROCK1 mice (Figures 4I).

Since Dynamin-related protein (Drp) 1 is a key component of the mitochondrial fission machinery (Jagasia et al., 2005), we tested whether the effect of ROCK1 on mitochondrial fission involved Drp1 activation. Mitochondrial recruitment of Drp1 appears to be required for its action on mitochondrial fission (Chang and Blackstone, 2010), therefore, we examined the possibility that ROCK1 mediates mitochondrial translocation of Drp1 in the diabetic milieu. We observed a marked increase in Drp1 in mitochondria-enriched fractions (mtDrp1) of the kidney glomeruli of wild-type diabetic mice (Figure 5A, **left panel, and** Figure S2-C). The increase in mitochondrial Drp1 levels was abolished in ROCK1$^{-/-}$ diabetic mice. Conversely, mtDrp1 was significantly increased in the kidney glomeruli of podocin Cre cA-ROCK1 mice (Figure 5A, **right panel, and** Figure S2-C), indicating that ROCK1 plays an important role in remodeling of mitochondrial morphology in podocytes, possibly by regulating Drp1 recruitment to the mitochondria *in vivo*.

ROCK1 Mediates Hyperglycemic-Induced mtROS and Apoptosis in Podocytes and Kidney Microvascular Endothelial Cells (mECs) in Vitro

We next studied the effects of ROCK1 on mtROS, cellular apoptosis, and mitochondrial fission in cultured cells. We focused on podocytes and endothelial cells because of strong

co-localization of ROCK1 with markers of podocytes and endothelial cells in the glomeruli (Figure S3-A). We simultaneously measured the effect of ROCK1 on mitochondrial superoxide production and apoptotic markers by flow cytometry in cultured podocytes and kidney microvascular endothelial cells (mECs) as previously described (Mukhopadhyay et al., 2007). The data in Figure 5B represent the distribution of non-apoptotic, apoptotic, and dead cells by Annexin V-FITC and Sytox Red staining and histogram analysis of mean intensity of oxidized MitoSOX Red in podocytes. Cells were separated into three groups: non-apoptotic cells (green), early apoptotic cells (purple), and dead cells (orange). The total fluorescence intensity of oxidized mitoSOX red measured by flow cytometry is depicted in light blue. High glucose stimulation (HG, 25mM for 24–36 hrs) increased the number of apoptotic cells ~4-fold (Figure 5C), and induced ~2.5-fold increase in the mtROS (Figure 5D) as measured by MitoSOX Red fluorescence intensity compared to that in normal glucose (NG, 5mM) in cultured podocytes. Next, we knocked down expression of ROCK1 with a specific ROCK1 siRNA (50nM, Figure S3-B) or used fasudil (10μmol/L) to assess the role of endogenous ROCK1. Knockdown of ROCK1 with siRNA or pharmacological inhibition of ROCK1 with fasudil significantly decreased the number of apoptotic cells (10±0.05 and 11%±0.8 *vs* 35±2%; $p<0.05$) and the production of mtROS (733±70 and 801±57 *vs.* 1459±73 mean fluorescence intensity, $p<0.05$) (Figures 5B, 5C, and 5D). These data suggest a critical role for ROCK1 activation in HG-induced mtROS production and cell apoptosis. Similar data were obtained in mECs (Figures S3-C, S4-A and S4-B).

To better understand the role of ROCK1 in HG-induced cellular apoptosis and its downstream signaling, we first examined the temporal profile of HG-induced ROCK1 activation in cultured podocytes and mECs. ROCK1 activity was significantly increased after 6 hrs with HG-treatment (25 mM) in both podocytes (Figure 5E) and mECs (Figure S5-A), suggesting that ROCK1 activation is an early response to HG stimulation. Mitochondrial fractionation experiments indicated that mtBax increased and cytochrome *c* decreased in cells upon their exposure to HG (Figures 5F, and 5G). However, ROCK1 knockdown prevented the effect of HG on mtBax and cytochrome *c*. Furthermore, knockdown of ROCK1 also reversed HG-induced caspase-3 activity in podocytes (Figure 5H), suggesting a critical role for ROCK1 in HG-induced mitochondrial apoptotic pathway, consistent with our *in vivo* studies. Similar results were obtained in mECs (Figures S5-B, S5-C, and S5-D). Conversely, cA-ROCK1 transfected-podocytes exhibited increased mtBax and caspase-3 activity and lower levels of cytochrome *c* in mitochondria (Figures 5I, and 5J).

ROCK1 Mediates Hyperglycemia-Induced Drp1 Recruitment to the Mitochondria

We next examined whether ROCK1 recruitment to the mitochondria was necessary for its effect on mitochondrial fission and increased ROS generation. We stimulated podocytes with HG as previously described and performed double immunofluorescence staining for ROCK1 and MitoTracker, a mitochondrial marker. ROCK1 did not co-localize to mitochondria in response to HG (25 mM for 18 hrs) and its protein expression was not detectable in the mitochondrial fractions from HG-stimulated podocytes *in vitro* or from kidney glomeruli obtained from STZ-induced diabetic mice *in vivo* (Figures S6-A, and S6-B). These observations suggest that the effect of ROCK1 on mtROS and apoptosis is not dependent on the recruitment of ROCK1 to the mitochondria.

Since Drp1 translocation to the mitochondria is a key event in mitochondrial fission (Jagasia et al., 2005; James and Martinou, 2008; Labrousse et al., 1999), we next tested the possibility that ROCK1 might exert its effect on mitochondrial fission by promoting Drp1 translocation to the mitochondria. We initially examined the effect of ROCK1 on subcellular distribution of Drp1. We observed that upon stimulation with HG, mitochondria became short and fragmented, whereas podocytes transfected with specific siROCK1 or siDrp1 maintained their elongated mitochondrial morphology in hyperglycemic conditions (Figures

6A, and 6B). We further observed that ROCK1 knockdown markedly reduced HG-induced Drp1 recruitment to the mitochondria in podocytes (Figures 6C, **and** S7-A) and in mECs (Figures S7-B, and S7-C), suggesting that ROCK1 may modulate mitochondrial fission through Drp1 translocation to the mitochondria. To confirm the effect of ROCK1 on mitochondrial dynamics, we next examined the effect of ROCK1 overexpression on mitochondrial fission. Whereas podocytes transfected with cA-ROCK1 exhibited more fragmented mitochondria with a marked increase in Drp1 recruitment to the mitochondria under normal glucose (NG, 5mM) conditions, this fragmented phenotype was reversed when Drp1 was knocked down by a lentiviral Drp1 short hairpin RNA (shRNA) (Figures 6D, 6E, 6-F, and S7-D). Notably, simultaneous analysis of measured superoxide production and apoptosis revealed that podocytes co-transfected with cA-ROCK1 and Drp1 shRNA had lower levels of mtROS and exhibited less cellular apoptosis (Figure 6G). Taken together, these data indicate that ROCK1 may promote mitochondrial fission, mtROS production, and cellular apoptosis through Drp1 translocation to the mitochondria.

ROCK1 Mediates Drp1 Recruitment to the Mitochondria by Phosphorylating Drp1 at Serine^{600} Residue

Because virtually nothing was known about the effect of ROCK1 on regulating subcellular localization of Drp1, we sought to define the regulatory mechanisms by which ROCK1 activated Drp1. We initially questioned whether ROCK1 can interact with Drp1 in response to HG stimulation in intact cells. Transfected mECs expressing Flag-Drp1, ROCK1, or co-expressing both plasmids were stimulated with HG (25 mM). Immunoprecipitation of cell lysates with an anti-Flag antibody, followed by Western blot analysis revealed that ROCK1 and Drp1 were co-immunoprecipitated when cells were treated with HG for 5 hrs (Figure 7A), indicating that ROCK1 and Drp1 are closely associated under hyperglycemic conditions.

The ability of ROCK1 to associate with Drp1, in response to hyperglycemic stimulation, led us to examine whether Drp1 might be a direct substrate of ROCK1. We tested the possibility that ROCK1, a serine/threonine kinase, can induce phosphorylation of Drp1 at a serine residue and whether serine phosphorylation of Drp1 could have mediated the effect of ROCK1 on Drp1 recruitment to the mitochondria. In support of our hypothesis, previous published work has shown that a series of kinases can influence subcellular localization of Drp1 by phosphorylating two main conserved serine residues of Drp1 (Chang and Blackstone, 2007b, 2010). Based on the consensus sequence motif of ROCK substrates (R/K-X-X-S/T or R/K-X-S/T where R is arginine; K, lysine; S, serine; and T; threonine) (Kang et al., 2007), we identified Ser^{600} in the mouse Drp1 isoform b as a potential phosphorylation site for ROCK1 (Figure 7B). This serine phosphorylation site is highly conserved among species and is located at the GTPase effector domain (GED) of Drp1 (Figure 7B). Using phospho-specific Drp1 antibodies, we observed that HG stimulation (25 mM for 36 hrs) increased phosphorylation of Drp1 at Ser^{600} (corresponding to Ser^{637} in human Drp1 isoform 1) (Figure 7C). ROCK1 knockdown, either by using dominant negative ROCK1 (dn ROCK1) or siROCK1, attenuated Drp1 phosphorylation at Ser^{600}, but not at Ser^{579}, another regulatory phosphoserine site of Drp1 (corresponding to Ser^{616} in human Drp1 isoform-1) (Figure 7C).

To determine whether Ser^{600} was the precise site for phosphorylation by ROCK1 *in vitro*, we performed an *in vitro* kinase assay using bacterially expressed Drp1 as a substrate for purified ROCK1. ROCK1 protein was labeled with [γ-^{32}P] ATP *in vitro*, and Drp1 phosphorylation was assessed in wild type Drp1 (wt Drp1) or a Drp1 mutant protein (S600A) where Ser^{600} was replaced with alanine. As shown in Figure 7D, we observed that ROCK1 was able to phosphorylate wt Drp1 protein, but not Drp1 S600A protein *in vitro*. These data indicate that ROCK1 specifically phosphorylates Drp1 at the Ser^{600} residue.

Having identified the site of ROCK1-induced Drp1 phosphorylation, we next assessed the contribution of Ser^{600} phosphorylation on Drp1 recruitment to the mitochondria. Two recent publications have provided seemingly contradictory data on the functional consequences of Drp1 phosphorylation at Ser^{600}. Whereas one study reported that phosphorylation of Drp1 at $Ser^{637/656}$ (human/rat) (corresponding to Ser^{600} in mouse Drp1 isoform b) decreased Drp1 recruitment to the mitochondria (Chang and Blackstone, 2007a), a more recent report demonstrated that phosphorylation of the same site in human Drp1 isoform 3 by the Ca^{2+}/calmodulin-dependent protein kinase Iα (CaMK1α) enhanced Drp1 recruitment to the mitochondria and increased mitochondrial Drp1 abundance (Han et al., 2008). We tested the effect of phosphorylation of Drp1 at Ser^{600} on its subcellular localization by transfecting podocytes with Flag-Drp1 (wt) or Flag-Drp1 S600A. We found that HG (25 mM for 36 hrs) induced a significant increase in Drp1 recruitment to the mitochondria, that was reduced in cells transfected with Drp1 S600A (Figure 7E), suggesting that ROCK1-mediated phosphorylation of Drp1 at Ser^{600} site promotes Drp1 translocation to the mitochondria. Furthermore, to assess the effect of Drp1 phosphorylation at Ser^{600} on mitochondrial fission, we knocked down endogenous Drp1 in podocytes using a lentiviral Drp1 shRNA, and analyzed the mitochondrial morphology in cells transfected with either an empty vector, wild type (wt) Drp1, or S600A mutant of Drp1. Whereas HG-induced cells transfected with Drp1 shRNA had long mitochondria, cells transfected with wt Drp1 exhibited short punctate mitochondria (Figures 7F, and S7-E). Conversely, cells transfected with Drp1 S600A exhibited a significant shift from the fragmented phenotype to elongated mitochondria (Figure 7F, **right panel)**, suggesting a direct effect of Drp1 phosphorylation at Ser^{600} on mitochondrial fission. Consistent with these results, Drp1 knockdown in HG-treated cells expressing Drp1 S600A decreased cellular apoptosis compared with cells expressing wt Drp1 (Figure 7G). Importantly, podocytes transfected with a phosphomimetic version of Drp1 (Drp1 S600D) showed a marked increase in mitochondrial fragmentation (Figure 7H). These gain-of-function experiments support the previously describe loss-of-function experiments, and indicate a critical role of ROCK1 in mitochondrial fission by promoting phosphorylation of Drp1 at Ser^{600}.

DISCUSSION

The role of ROCK1 isoform in the pathogenesis of DN is unknown. Furthermore, almost nothing is known about the effect of ROCK1 on mitochondrial remodeling or the molecular mechanisms by which ROCK1 could potentially modulate mitochondrial dynamics. In order to address these questions, we generated two diabetic ROCK1 knockout mice and an inducible podocyte-specific ROCK1 knock-in mouse model to study the specific role of ROCK1 and its downstream signaling on mitochondrial fission and on progression of DN. Our results indicate that diabetic ROCK1 null mice exhibit significant reduction in albuminuria, while inducible podocyte-specific cA-ROCK1 knock-in mice had higher levels of albuminuria. We identified Drp1 as a direct substrate for ROCK1, and provide the evidence that ROCK1-mediated phosphorylation of Drp1 at Ser^{600} contributes to enhanced mitochondrial fission.

Mitochondrial fission has been previously implicated as a critical mediator of increased ROS production in hyperglycemic conditions (Brooks et al., 2009), but the key signaling events linking hyperglycemia with increased mitochondrial ROS production have remained elusive. We now report that hyperglycemia-induced mitochondrial fission depends on both ROCK1 activation and Drp1 translocation to the mitochondria. This ROCK1-dependent metabolic pathway involves phosphorylation of Drp1 at Ser600, which promotes its recruitment to the mitochondria. These findings provide a clear link between hyperglycemia and increased ROS generation *via* a previously unrecognized signaling pathway, which

involves ROCK1 activation, Drp1 phosphorylation, and Drp1 recruitment to the mitochondria leading to increased mitochondrial fission and cellular apoptosis.

Drp1 phosphorylation is one of the key regulatory post-translational modifications of Drp1, which modulates its translocation to the mitochondria (Chang and Blackstone, 2007b; Cribbs and Strack, 2007). However, despite the central importance of Drp1 phosphorylation in mitochondrial fission, the functional consequences of the two conserved serine phosphorylation sites on Drp1 activation remain incompletely understood. For example, while PKA phosphorylation of Drp1 at $Ser^{637/656}$ (human/rat) decreases Drp1 GTPase activity (Chang and Blackstone, 2007a; Cribbs and Strack, 2007), but phosphorylation of the same conserved serine residue in Drp1 isoform3 by Ca^{2+}/calmodulin-dependent protein kinase Iα (CaMKIα) causes a significant increase in Drp1 recruitment to the mitochondria (Han et al., 2008). Our interpretation of these seemingly contradictory observations is that the functional consequences of serine phosphorylation of Drp1 could be highly cell-type and/or stimulus dependent. In our experimental models, ROCK1-mediated Ser^{600} phosphorylation (mouse Drp1 isoform b) resulted in Drp1 translocation to the mitochondria, similar to the effect of (CaMKIα) leading to enhanced cellular apoptosis. These findings, nevertheless, do not exclude that other ROCK1-dependent pathways, independent of Drp1 phosphorylation, may also play important roles in the ROCK1-mediated cellular response to metabolic stress, and they do not exclude that the effect ROCK1 on progression of DN may be mediated, at least in part, through other pathways.

Collectively, the findings of this study provide significant insights into the pathobiology of ROCK1 in the diabetic milieu. First, we propose a role for ROCK1 in hyperglycemic-induced mitochondrial fission. Second, we identify Drp1 as a direct substrate for ROCK1. Third, we identify the precise ROCK1-mediated phosphorylation site of Drp1; and finally, we provide direct evidence for a role of ROCK1 in progression of DN. These findings demonstrate an unexpected role for ROCK1 in mitochondrial fission. Although the expression of ROCK2 in $ROCK1^{-/-}$ glomeruli was unaltered, a role for ROCK2 on mitochondrial dynamics cannot be completely ruled out.

In conclusion, our findings define a metabolic pathway by which ROCK1 activation promotes mitochondrial fragmentation under high glucose conditions, and provide insights into the role of ROCK1 in a signaling cascade involving Drp1 activation and mitochondrial remodeling.

EXPERIMENTAL PROCEDURES

Animals

All animal studies were carried out with approval of the Institutional Animal Care and Use Committee (IACUC) of Baylor College of Medicine. Generation and characterization of $ROCK1^{-/-}$ mice have been previously described (Zhang et al., 2006). Since db/db mice are infertile, to generate db/db:$ROCK1^{-/-}$ double mutant mice, FVB *db*/+ (Jackson Laboratory Bar Harbor, ME) mice were initially mated with FVB $ROCK^{-/-}$ mice, and then db/+:$ROCK1^{+/-}$ were crossed with $ROCK1^{-/-}$ mice, and finally db/+:$ROCK1^{-/-}$ mice were intercrossed to generate db/db:$ROCK1^{-/-}$ double mutant mice. To create an inducible constitutively active (cA) ROCK1 knock-in mouse, a cA mutant of ROCK1 (human Δ3 cA-ROCK1) was used to generate the cA-ROCK1 knock-in targeting vector (Fujisawa et al., 1996). The ubiquitin C promoter was used to drive cA-ROCK1 cDNA expression only when the loxP-stop-loxP is removed. A Neo cassette driven by a PGK promoter was used to facilitate selection of positive ES cell clones. FRT sequences were recognized by FLP recombinase. We generated chimaeras by blastocyst injection of ES cells. After germline

transmission, the mice were crossed to C57BL/6J mice expressing FLP recombinase to remove the neo cassette.

Plasmid DNA and siRNA

Mouse Drp1 S600A and S600D mutations were achieved by using PCR-based mutagenesis with the following primers respectively: CCAGTTG CAAGAAAGCTAGCTGCCCGAGAACAGCGAGAT (Forward) and AAAACTGGAT GCCCGAGAACAG (Reverse). C-terminal mouse Drp1 (isoform b, 490–699) was amplified by PCR from the cDNA clone (Open Biosystems) using the following primer set: GTGAATTCGAGCTAGCGTATATCAACACAAAACACCCC (forward) and AGG GATCCTCACCAAAGATGAGTCTCTCGGATTTCAGC (reverse), and subcloned between EcoRI and BamHI sites of pGTK3XF vector. siRNAs for ROCK1, Drp1, Bax and scramble siRNA controls were purchased from Thermo Scientific (Chicago, IL). Transfections were performed using Lipofectamine 2000™ (Invitrogen, Carlsbad, CA) according to manufacturer's protocols.

Generation of Drp1-knockdown stable cells

Mouse Drp1 shRNA lentiviral particle and the scramble shRNA lentiviral particle were purchased from Santa Cruz Biotechnology. These viral particles were used to infect undifferentiated podocytes with 8 μg/ml polybrene (Sigma) and were subsequently selected with 2 μg/ml puromycin (Sigma) in the presence of 20 U/ml IFN-γ at 33°C.

In vitro kinase assay

Recombinant GST-Drp1 proteins were purified using glutathione sepharose (GE Healthcare) according to the manufacturer's protocol, and digested with PreScission protease (GE Healthcare) to remove the GST-tag. 1 μg of Drp1 wild-type or S600A mutant was incubated with 0.1 μg purified active ROCK1 (GST fusion of amino acid 17–535 of human ROCK1, Abcam) in a 30 μl reaction buffer [25 mM Tris (pH 7.5), 10 mM $MgCl_2$, 0.5 mM EGTA, 0.5 mM Na_3VO_4, 5 mM β-glycerophosphate, 2.5 mM DTT, 0.01% Triton X-100, 100 μM ATP and 10 μCi [γ-^{32}P]-ATP. After 30min incubation at 37°C, reactions were stopped by adding SDS sample buffer to 1X and separated by 12% SDS-PAGE.

Flow cytometry

Detection of apoptosis and mitochondrial superoxide production was performed as previously described (Mukhopadhyay et al., 2007). Samples were analyzed using BD FACSCantoII flow cytometer (BD Biosciences, CA) at the BCM Cell Sorting Facility.

Mitochondrial fragmentation

The Aspect ratio was calculated as previously described (Brooks et al., 2009; Brooks et al., 2007; Yu et al., 2006).

Statistical analysis

The data are summarized as the mean ± SEM. Statistical significance was assessed by performing analysis of variance (ANOVA) followed by the Tukey-Kramer post hoc analysis for multiple comparisons using an α value of 0.05 in GraphPad Prism software (San Diego, CA).

Supplementary Material

Refer to Web version on PubMed Central for supplementary material.

Acknowledgments

This work was supported by National Institutes of Health grant RO1DK078900 and R01 RO1DK091310 to FRD. We thank Craig Blackstone, M.D., Ph.D (NIH, Bethesda, MD) for providing anti-phospho Drp1 antibody, Ah-Lim Tsai, M.D., Ph.D. (University of Texas at Houston) for his help with EPR spectroscopy, and Lei Wei, PhD (University of Indiana) for providing ROCK1 constructs.

References

1. Brooks C, Wei Q, Cho SG, Dong Z. Regulation of mitochondrial dynamics in acute kidney injury in cell culture and rodent models. J Clin Invest. 2009; 119:1275–1285. [PubMed: 19349686]
2. Brooks C, Wei Q, Feng L, Dong G, Tao Y, Mei L, Xie ZJ, Dong Z. Bak regulates mitochondrial morphology and pathology during apoptosis by interacting with mitofusins. Proc Natl Acad Sci U S A. 2007; 104:11649–11654. [PubMed: 17606912]
3. Brownlee M. Biochemistry and molecular cell biology of diabetic complications. Nature. 2001; 414:813–820. [PubMed: 11742414]
4. Chang CR, Blackstone C. Cyclic AMP-dependent protein kinase phosphorylation of Drp1 regulates its GTPase activity and mitochondrial morphology. J Biol Chem. 2007a; 282:21583–21587. [PubMed: 17553808]
5. Chang CR, Blackstone C. Drp1 phosphorylation and mitochondrial regulation. EMBO J. 2007b; 8:1088–1089.
6. Chang CR, Blackstone C. Dynamic regulation of mitochondrial fission through modification of the dynamin-related protein Drp1. Ann N Y Acad Sci. 2010; 1201:34–39. [PubMed: 20649536]
7. Chang J, Xie M, Shah VR, Schneider MD, Entman ML, Wei L, Schwartz RJ. Activation of Rho-Associated Coiled-Coil Protein Kinase 1 (ROCK-1) by Caspase-3 Cleavage Plays an Essential Role in Cardiac Myocyte Apoptosis. Proc Natl Acad Sci U S A. 2006; 103:14495–14500. [PubMed: 16983089]
8. Chow FY, Nikolic-Paterson DJ, Ozols E, Atkins RC, Rollin BJ, Tesch GH. Monocyte chemoattractant protein-1 promotes the development of diabetic renal injury in streptozotocin-treated mice. Kidney Int. 2006; 69:73–80. [PubMed: 16374426]
9. Coughlan MT, Thallas-Bonke V, Pete J, Long DM, Gasser A, Tong DCK, Arnstein M, Thorpe SR, Cooper ME, Forbes JM. Combination Therapy with the Advanced Glycation End Product Cross-Link Breaker, Alagebrium, and Angiotensin Converting Enzyme Inhibitors in Diabetes: Synergy or Redundancy? Endocrinology. 2007; 148:886–895. [PubMed: 17110423]
10. Cribbs JT, Strack S. Reversible phosphorylation of Drp1 by cyclic AMP-dependent protein kinase and calcineurin regulates mitochondrial fission and cell death. EMBO Rep. 2007; 8:939–944. [PubMed: 17721437]
11. Davies SP, Reddy H, Caivano M, Cohen P. Specificity and mechanism of action of some commonly used protein kinase inhibitors. Biochem J. 2000; 351:95–105. [PubMed: 10998351]
12. de Cavanagh EMV, Ferder Ln, Toblli JE, Piotrkowski Br, Stella Is, Fraga CG, Inserra F. Renal mitochondrial impairment is attenuated by AT1 blockade in experimental Type I diabetes. American Journal of Physiology - Heart and Circulatory Physiology. 2008; 294:H456–H465. [PubMed: 18024545]
13. Fujisawa K, Fujita A, Ishizaki T, Saito Y, Narumiya S. Identification of the Rho-binding Domain of p160ROCK, a Rho-associated Coiled-coil Containing Protein Kinase. J Biol Chem. 1996; 271:23022–23028. [PubMed: 8798490]
14. Gojo A, Utsunomiya K, Taniguchi K, Yokota T, Ishizawa S, Kanazawa Y, Kurata H, Tajima N. The Rho-kinase inhibitor, fasudil, attenuates diabetic nephropathy in streptozotocin-induced diabetic rats. Eur J Pharmacol. 2007; 568:242–247. [PubMed: 17511984]
15. Han XJ, Lu YF, Li SA, Kaitsuka T, Sato Y, Tomizawa K, Nairn AC, Takei K, Matsui H, Matsushita M. CaM kinase I{alpha}–induced phosphorylation of Drp1 regulates mitochondrial morphology. J Cell Biol. 2008; 182:573–585. [PubMed: 18695047]
16. Haudek SB, Gupta D, Dewald O, Schwartz RJ, Wei L, Trial J, Entman ML. Rho kinase-1 mediates cardiac fibrosis by regulating fibroblast precursor cell differentiation. Cardiovasc Res. 2009; 83:511–518. [PubMed: 19406912]

17. Jagasia R, Grote P, Westermann B, Conradt B. DRP-1-mediated mitochondrial fragmentation during EGL-1-induced cell death in C. elegans. Nature. 2005; 433:754–760. [PubMed: 15716954]
18. James DI, Martinou JC. Mitochondrial dynamics and apoptosis: a painful separation. Dev Cell. 2008; 15:341–343. [PubMed: 18804432]
19. Kang JH, Jiang Y, Toita R, Oishi J, Kawamura K, Han A, Mori T, Niidome T, Ishida M, Tatematsu K, et al. Phosphorylation of Rho-associated kinase (Rho-kinase/ROCK/ROK) substrates by protein kinases A and C. Biochimie. 2007; 89:39–47. [PubMed: 16996192]
20. Kikuchi Y, Yamada M, Imakiire T, Kushiyama T, Higashi K, Hyodo N, Yamamoto K, Oda T, Suzuki S, Miura S. A Rho-kinase inhibitor, fasudil, prevents development of diabetes and nephropathy in insulin-resistant diabetic rats. J Endocrinol. 2007; 192:595–603. [PubMed: 17332527]
21. Kiritoshi S, Nishikawa T, Sonoda K, Kukidome D, Senokuchi T, Matsuo T, Matsumura T, Tokunaga H, Brownlee M, Araki E. Reactive Oxygen Species from Mitochondria Induce Cyclooxygenase-2 Gene Expression in Human Mesangial Cells. Diabetes. 2003; 52:2570–2577. [PubMed: 14514642]
22. Kolavennu V, Zeng L, Peng H, Wang Y, Danesh FR. Targeting of RhoA/ROCK signaling ameliorates progression of diabetic nephropathy independent of glucose control. Diabetes. 2008; 57:714–723. [PubMed: 18083785]
23. Labrousse AM, Zappaterra MD, Rube DA, van der Bliek AM. C. elegans Dynamin-Related Protein DRP-1 Controls Severing of the Mitochondrial Outer Membrane. Mol Cell. 1999; 4:815–826. [PubMed: 10619028]
24. Mukhopadhyay P, Rajesh M, Hasko G, Hawkins BJ, Madesh M, Pacher P. Simultaneous detection of apoptosis and mitochondrial superoxide production in live cells by flow cytometry and confocal microscopy. Nat Protoc. 2007; 2:2295–2301. [PubMed: 17853886]
25. Nishikawa T, Edelstein D, Du XL, Yamagishi S, Matsumura T, Kaneda Y, Yorek MA, Beebe D, Oates PJ, Hammes HP, et al. Normalizing mitochondrial superoxide production blocks three pathways of hyperglycaemic damage. Nature. 2000; 404:787–790. [PubMed: 10783895]
26. Noma K, Rikitake Y, Oyama N, Yan G, Alcaide P, Liu PY, Wang H, Ahl D, Sawada N, Okamoto R, et al. ROCK1 mediates leukocyte recruitment and neointima formation following vascular injury. J Clin Invest. 2008; 118:1632–1644. [PubMed: 18414683]
27. Ongusaha PP, Qi HH, Raj L, Kim YB, Aaronson SA, Davis RJ, Shi Y, Liao JK, Lee SW. Identification of ROCK1 as an upstream activator of the JIP-3 to JNK signaling axis in response to UVB damage. Sci Signal. 2008; 1:ra14. [PubMed: 19036714]
28. Peng F, Wu D, Gao B, Ingram AJ, Zhang B, Chorneyko K, McKenzie R, Krepinsky JC. RhoA/Rho-kinase contribute to the pathogenesis of diabetic renal disease. Diabetes. 2008; 57:1683–1692. [PubMed: 18356410]
29. Piskernik C, Haindl S, Behling T, Gerald Z, Kehrer I, Redl H, Kozlov AV. Antimycin A and lipopolysaccharide cause the leakage of superoxide radicals from rat liver mitochondria. Biochim Biophys Acta. 2008; 1782:280–285. [PubMed: 18298959]
30. Pospisilik JA, Knauf C, Joza N, Benit P, Orthofer M, Cani PD, Ebersberger I, Nakashima T, Sarao R, Neely G, et al. Targeted deletion of AIF decreases mitochondrial oxidative phosphorylation and protects from obesity and diabetes. Cell. 2007; 131:476–491. [PubMed: 17981116]
31. Riento K, Ridley AJ. Rocks: multifunctional kinases in cell behaviour. Nat Rev Mol Cell Biol. 2003; 4:446–456. [PubMed: 12778124]
32. Rube DA, van der Bliek AM. Mitochondrial morphology is dynamic and varied. Mol Cell Biochem. 2004:256–257. 331–339.
33. Sasaki Y, Suzuki M, Hidaka H. The novel and specific Rho-kinase inhibitor (S)-(+)-2-methyl-1-[(4-methyl-5-isoquinoline)sulfonyl]-homopiperazine as a probing molecule for Rho-kinase-involved pathway. Pharmacol Ther. 2002; 93:225–232. [PubMed: 12191614]
34. Tanaka A, Youle RJ. A chemical inhibitor of DRP1 uncouples mitochondrial fission and apoptosis. Mol Cell. 2008; 29:409–410. [PubMed: 18313377]
35. Wang J, Wang Y, Long J, Chang BH, Wilson MH, Overbeek P, Danesh FR. Tamoxifen-inducible podocyte-specific iCre recombinase transgenic mouse provides a simple approach for modulation of podocytes in vivo. Genesis. 2010; 48:446–451. [PubMed: 20641128]

36. Youle RJ, Karbowski M. Mitochondrial fission in apoptosis. Nat Rev Mol Cell Biol. 2005; 6:657–663. [PubMed: 16025099]

37. Yu T, Robotham JL, Yoon Y. Increased production of reactive oxygen species in hyperglycemic conditions requires dynamic change of mitochondrial morphology. Proc Natl Acad Sci U S A. 2006; 103:2653–2658. [PubMed: 16477035]

38. Zhang YM, Bo J, Taffet GE, Chang J, Shi J, Reddy AK, Michael LH, Schneider MD, Entman ML, Schwartz RJ, et al. Targeted deletion of ROCK1 protects the heart against pressure overload by inhibiting reactive fibrosis. FASEB J. 2006; 20:916–925. [PubMed: 16675849]

HIGHLIGHTS

1. ROCK1 is a potent regulator of mitochondrial dynamics in diabetic nephropathy.
2. Drp1 is a direct substrate for ROCK1 in the diabetic milieu.
3. ROCK1 triggers mitochondrial fission by phosphorylating Drp1 at Serine 600.
4. Podocyte-specific ROCK1 activation promotes mitochondrial fission in mice.

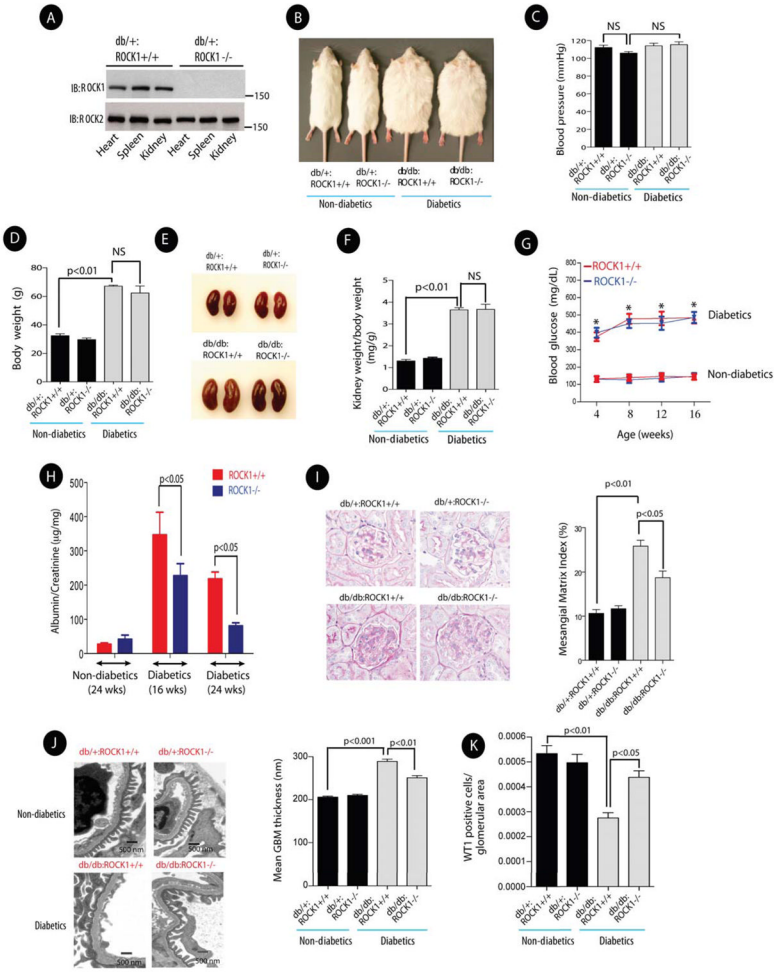

Figure 1. Deletion of ROCK1 Significantly Reduced Albuminuria, and Mesangial Matrix Expansion in the Kidneys of db/db Mice

(A) A representative Western blot confirming deletion of ROCK1 in several tissues in $Lepr^{db/+}$:$ROCK1^{-/-}$ mice ***(upper panel)***. ROCK2 expression levels were unchanged in the same tissues ***(lower panel)***. **(B)** Representative pictures of mice in each group at 24-weeks of age. **(C)** Systolic blood pressure and body weight **(D)** were measured in 24-week-old mice in each group. NS: Not significant. **(E)** Representative images of kidneys obtained from 24 weeks old mice. **(F)** Kidney weight/body weight ratio in each group. **(G)** Blood glucose levels in each group. *represents significant statistical differences between diabetics and non-diabetics mice ($p<0.01$). **(H)** Urinary albumin excretion was measured at 16-weeks and 24 weeks of age. **(I)** Representative images of Periodic Acid Schiff (PAS) staining of kidney sections ***(left panel)*** (original magnification, x400), and quantification of Mesangial Matrix Index in each group ***(right panel)***. **(J)** Representative electron photomicrographs of glomerular basement membrane (GBM) thickening ***(left panel)***, and quantification of GBM thickness in each group ***(right panel)***. **(K)** Podocyte numbers were quantified by assessing nuclear WT1 staining in 50 randomly selected kidney glomeruli per animal in each group. Results are presented as mean±SE (n=5–8/group) in all figures, and analyzed by one-way ANOVA.

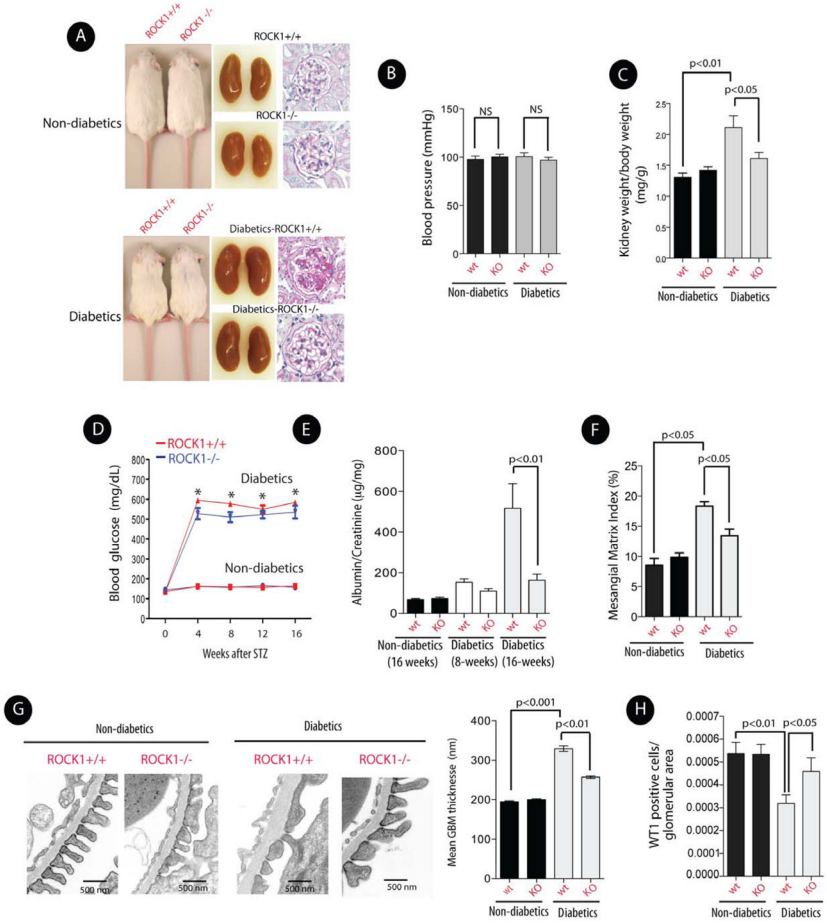

Figure 2. Deletion of ROCK1 Ameliorated Albuminuria in STZ-Induced Diabetic Mice

(A) Representative images of mice ***(left panel)***, kidneys ***(middle panel)***, and histology ***(right panel)*** of non-diabetic and diabetic ROCK1$^{-/-}$ and ROCK1$^{+/+}$ mice. Histological analysis was assessed by PAS staining (original magnification, x400). **(B)** Systolic blood pressure and kidney weight/body weight ratio **(C)** in 24-week-old mice in each group. **(D)** Blood glucose levels in each group. *represents significant statistical differences between diabetics and non-diabetics mice ($p<0.01$). **(E)** Albumin/creatinine ratio was measured in mice after 8 and 16 weeks of persistent hyperglycemia. **(F)** Mesangial Matrix Index was measured in each group. **(G)** Representative electron photomicrographs of GBM thickening ***(left panel)***, and quantification of GBM thickness in each group ***(right panel)***. **(H)** Podocyte numbers were quantified by assessing nuclear WT1 staining in each group. All data are presented as means ± SEM (n=8–12/each group), and analyzed by one-way ANOVA.

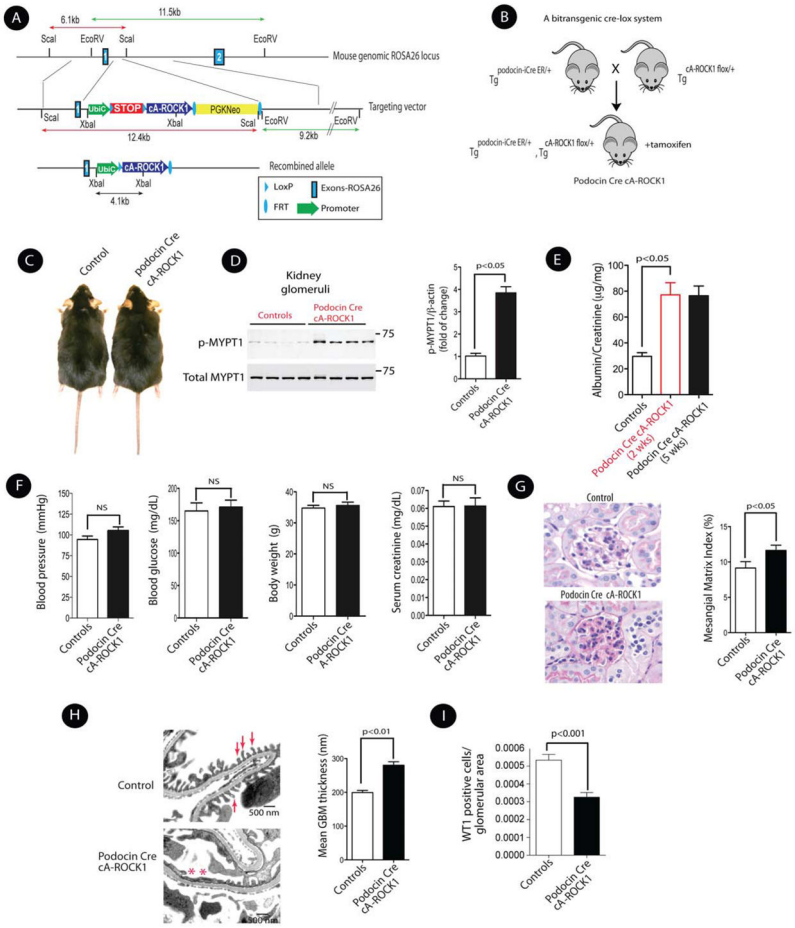

Figure 3. Generation and Initial Characterization of Inducible Podocin Cre cA-ROCK1 Knock-In Mice

(A) The schematic diagram illustrates the ROSA26 targeting locus, cA-ROCK1 targeting construct, and the conditional allele after homologous recombination. The ubiquitin C promoter (UbiC; green arrow) was used to drive constitutively active ROCK1 cDNA (cA-ROCK1; blue arrow) expression. (**B**) Breeding scheme of bitransgenic podocin Cre cA-ROCK1 mice. (**C**) Gross appearances of control and inducible podocin Cre cA-ROCK1 knock-in mice. (**D**) ROCK1 activity in the kidney glomeruli was performed by assessing p-MYPT in podocin Cre cA-ROCK1 knock-in mice (***left panel***). Quantitation of phospho-myosin phosphatase target subunit 1 (p-MYPT1) in each group (***right panel***). (**E**) Albumin/ creatinine ratio in podocin Cre cA-ROCK1 knock-in mice at 2 and 5 weeks post tamoxifen injection. **(F)** Systolic blood pressure, blood glucose, body weights and serum creatinine were assessed in podocin Cre cA-ROCK1 mice. **(G)** Photomicrographs of PAS staining from glomeruli of podocin Cre cA-ROCK1 (original magnification, x400) (***left panel***), and quantification of Mesangial Matrix Index in each group (***right panel***). **(H)** Representative electron micrographs of kidneys (***left panel***), and quantification of mean GBM in each group (***right panel***). Foot processes are indicated by arrows, and effacement of these processes are indicated by asterisks. **I)** Podocyte numbers were quantified in each group as previously described. All data are presented as means ± SEM (n=4–10/each group), and analyzed by one-way ANOVA.

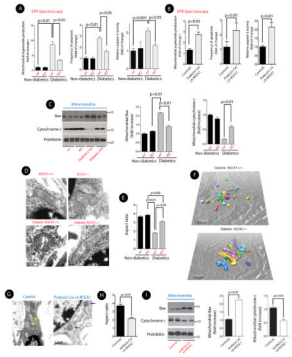

Figure 4. Deletion of ROCK1 Prevents Mitochondrial Fission, mtROS, and Glomerular Apoptosis

(A) Quantitative measurement of superoxide generation in isolated mitochondria from kidney glomeruli by EPR spectroscopy ***(left panel)***. Bar graph summarizing the number of apoptotic cells in glomeruli per 50 glomeruli counted in each group ***(middle panel)***. Bar graph summarizing caspase-3 activity in kidney glomeruli in different groups ***(right panel)***. **(B)** Quantitative measurement of superoxide generation ***(left panel)***, frequency of apoptosis ***(middle panel),*** and caspase-3 activity in isolated mitochondria from kidney glomeruli from podocin Cre cA-ROCK1 mice by EPR spectroscopy. **(C)** Representative Western blots (***left panel***) and bar graphs of Bax **(*middle panel*)** and cytochrome *c* **(*right panel*)**) of mitochondrial fractions obtained from kidney glomeruli in each group. All data are presented as means ± SEM (n=8–12/each group), and analyzed by one-way ANOVA. **(D)** Representative 2D-EM micrographs of mitochondria in podocytes from each group. (**E**) Quantification of mitochondrial Aspect ratio in podocytes. A total of 150 mitochondria in each group from 4 different animals were evaluated. **(F)** Representative 3D-EM images of mitochondria in podocytes from STZ-induced diabetic $ROCK^{+/+}$ and diabetic $ROCK^{-/-}$ mice. **(G)** Representative micrographs of mitochondrial morphology in podocytes from a control and a podocin Cre cA-ROCK1 knock-in mouse. **(H)** Quantification of mitochondrial Aspect ratio from **4G. (I)** Representative Western blots of mitochondrial Bax (mtBax) and cytochrome *c* (***left panel***) obtained from kidney glomeruli in each group. Quantification of mtBax (***middle panel***) and cytochrome *c* (***right panel***) from three independent experiments. All data are presented as means ± SEM (n=4–10/each group), unless stated otherwise, and analyzed by one-way ANOVA.

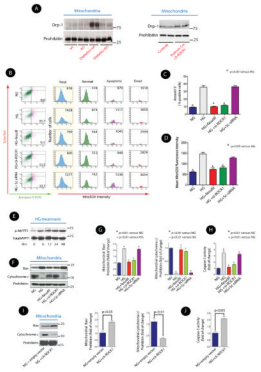

Figure 5. ROCK1 Modulates HG-Induced mtROS Production and Podocytes Apoptosis

(A) Representative Western blots of mitochondrial Drp1 from kidney glomeruli obtained from diabetic ROCK1$^{+/+}$ and ROCK1$^{-/-}$ mice ***(left panel)***, and from kidney glomeruli of podocin Cre cA-ROCK1 knock-in mouse ***(Right panel)***. **(B)** Representative histograms of flow cytometry experiments depicting simultaneous detection of apoptosis and mitochondrial superoxide production in live cultured podocytes. The changes in the number of apoptotic cells (% Annexin V-FITC positive), and superoxide production (MitoSOX Red) fluorescence intensity in total (blue), normal (green), apoptotic (purple) and dead (orange) cells are depicted in each condition following HG treatment for 24 hrs. Sc-siRNA: scrambled siRNA. Results are **(C)** Quantitative data expressing % of Annexin V-FITC positive cells and **(D)** mean fluorescence intensity of MitoSOX Red in response to HG in different conditions. **(E)** Representative Western blot of temporal profile of ROCK1 activity in HG (25 mM) treated podocytes. **(F)** Representative Western blots of mitochondrial Bax and cytochrome *c* in the cultured mouse podocyte in different conditions. **(G)** Quantitative analysis of mitochondrial Bax and cytochrome *c* from three independent experiments. **(H)** Quantitative changes in caspase-3 activity from three independent experiments. **(I)** Representative Western blots of mitochondrial Bax and cytochrome *c* in cA-ROCK1 transfected cultured podocytes. **(J)** Quantitative changes of caspase-3 activity in cA-ROCK1 transfected podocytes. The data are presented as means ± SEM of at least three independent experiments, unless stated otherwise, and analyzed by one-way ANOVA.

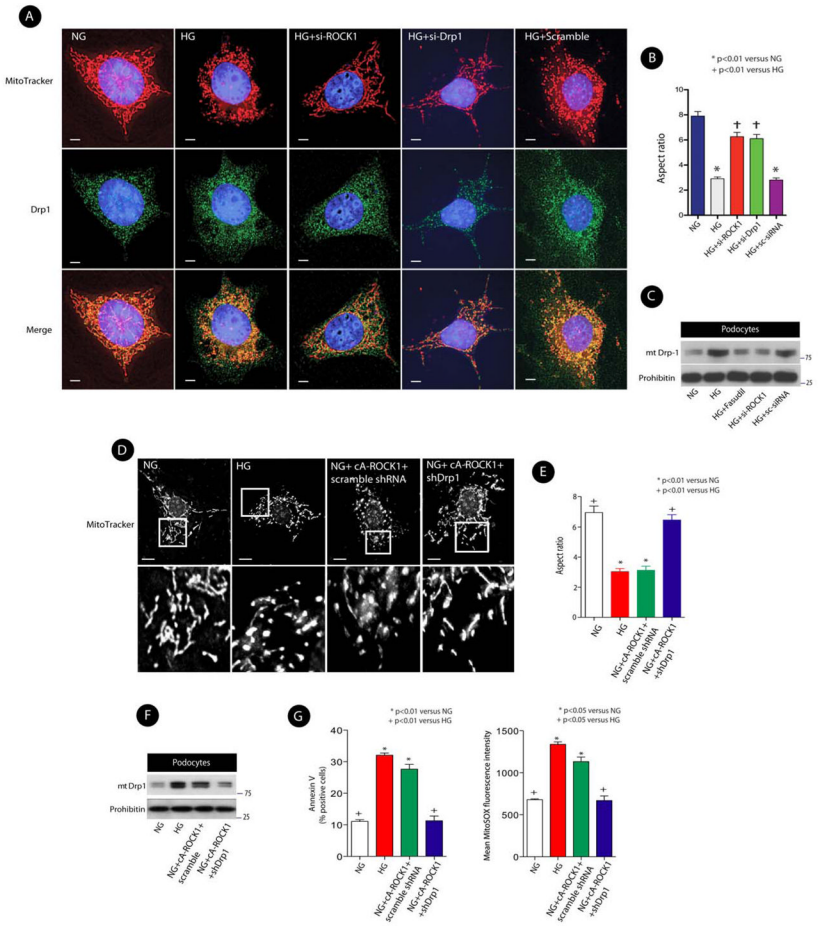

Figure 6. ROCK1 Mediates HG-Induced Mitochondrial Fission

(A) Double immunofluorescence of MitoTracker and Drp1 using deconvolution microscopy. Cells were transfected with scrambled siRNA, si-Drp1, or si-ROCK1. MitoTracker:red; DAPI:blue; Drp1:green, and merge: yellow. Magnification×1000. Scale bars, 5 μm. **(B)** Mitochondrial morphology was assessed by Aspect ratio analysis. The morphology of at least 120 mitochondria was determined in a triplicate and blinded manner. **(C)** Representative immunoblot analysis of mitochondrial Drp1 (mtDrp1) in cultured mouse podocytes transfected with si-ROCK1, scrambled (Sc) siRNA, or treated with fasudil (10 μmol/l). **(D)** Micrographs of mitochondrial morphology visualized by MitoTracker red staining of podocytes transfected with cA-ROCK1, Drp1 shRNA, or scramble shRNA. Scale bars, 15 μm. **(E)** Mitochondrial morphology was assessed by Aspect ratio from three independent experiments (>100 mitochondria). **(F)** Representative Western blot of mitochondrial Drp1 (mtDrp1) in cultured mouse podocytes transfected with cA-ROCK1, Drp1 shRNA, or scrambled (sc) shRNA. **(G)** Quantitative data expressing % of Annexin V-FITC positive cells ***(left panel)*** and MitoSOX Red ***(right panel)*** in different conditions. In all figures, the means ± SEM of at least three independent experiments and analyzed by one-way ANOVA are shown.

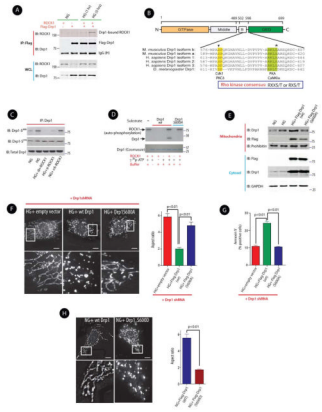

Figure 7. ROCK1 Promotes Mitochondrial Fission via Drp1 Phosphorylation at Ser^{600}

(A) Western blots of immunoprecipitates with anti-Flag antibody (IP) and whole cell lysates (WCL) of ROCK1 and Flag-Drp1 immunoblotted with anti-ROCK1 or anti-Drp1 antibodies in mECs treated with normal glucose (NG, 5 mM) or high glucose (HG, 25 mM) for 1 and 5 hrs. **(B)** Domain structure of mouse Drp1 isoform b. Sequences from several Drp1 isoforms were aligned to show the conserved motifs for Cdk1/PKCδ phosphorylation (inverted triangle) and PKA/CaMK1α phosphorylation (asterisk) sites. **(C)** Western blots of phospho-Drp1 (S^{600} and S^{579}) and total Drp1. **D)** *In vitro* kinase assay of bacterially expressed wild-type C-terminal Drp1 (490–699) and its mutant S600A by ROCK1 in the presence of [γ-^{32}P] ATP. Coomassie blue staining of Drp1 was used as the input loading control. **(E)** Western blots of mitochondrial and cytosolic fractions of Drp1 in mECs following transfection with Flag-Drp1 (wt) or Flag-Drp1 S600A, and exposed to HG (25 mM) for 36 hrs. **(F)** Micrographs of mitochondrial morphology visualized by MitoTracker red staining of podocytes expressing the indicated shRNAs and the transgenes. Scale bars, 15 μm. The bottom images show magnifications of the areas outlined in the top images. Quantification of mitochondrial Aspect ratio from three independent experiments (>100 mitochondria) ***(right panel).*** **(G)** Quantitative data expressing % of Annexin V-FITC positive cells in different conditions. **(H)** Mitochondrial morphology was visualized by MitoTracker red staining of podocytes expressing a Flag-wild type Drp1, or Flag Drp1S600D ***(left panel)***. The bottom images show magnifications of the areas outlined in the images above. Quantification of mitochondrial Aspect ratio from three independent experiments (>100 mitochondria) ***(right panel).*** Results are presented as means ± SEM of at least three independent experiments, and analyzed by one-way ANOVA.